Chapter 2

Synthesis and Characterization Techniques

2.1 Introduction

In this chapter, we describe the details of materials synthesis conditions and process optimization for preparation of various photovoltaic, ferroelectric samples investigated in the present thesis. The methods used for bulk and thin film sample preparation are discussed. The photovoltaic device fabrication and its characterization procedure is also discussed systematically. This chapter also introduces the brief principles of characterization techniques used in the present Ph.D. thesis.

2.2 Synthesis of Samples

In the present thesis, bulk and thin film samples of various ferroelectric solids solution compositions have been prepared using different methods. Mechano-chemical solid-state ceramic method has been used to prepare various compositions of ferroelectric solid solutions $xPbTiO_3$-$(1-x)Bi(Ni_{2/3}Nb_{1/3})O_3$, $(1-x)Bi(Co_{1/2}Ti_{1/2})O_3$–$xPbTiO_3$, $(1-x)$ $Bi(Ni_{2/3}Nb_{1/3})O_3$-$xBaTiO_3$, $(1-x)KNbO_3$-$xBa(Ni_{1/2}Nb_{1/2})O_3$ investigated in the present thesis. Thin film samples of xPbTiO$_3$–$(1–x)Bi(Ni_{2/3}Nb_{1/3})O_{34}$ has been grown on various substrates under optimized conditions by Pulse Laser Deposition (PLD) using the dense sintered pellets prepared by solid state ceramic method. In addition thin films of two compositions $0.60PbTiO_3$-$0.40Bi(Co_{0.60}Ti_{0.40})O_3$, $0.90KNbO_3$-$0.10Ba(Ni_{1/2}Nb_{1/2})O_3$ has been grown by RF Magnetron sputtering using sintered pellets prepared by solid state ceramic method. Thin film of one composition $0.90KNbO_3$-$0.10Ba(Ni_{1/2}Nb_{1/2})O_3$ has been prepared by Sol-gel spin coating. To illustrate and discuss various steps followed during solid state ceramic sample preparation, we will take $xPbTiO_3$-$(1-x)Bi(Ni_{2/3}Nb_{1/3})O_3$ (xPT-(1-x)BNNO) as the representative system. Fig. 2.1 shows the schematic illustration of steps involved in getting phase pure solid solutions by Mechano-chemical solid-state ceramic method.

This sequence of synthesis steps is adopted to avoid the formation of impurities in various compositions as described in the following sections.

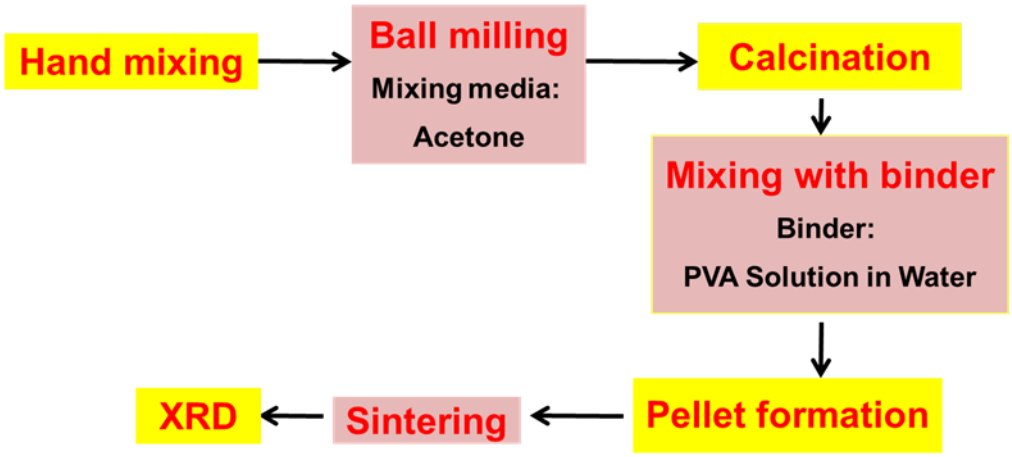

Figure 2.1 Schematic illustrations of steps of synthesis process to get phase pure ferroelectric perovskite solid solution using Mechano-chemical solid-state ceramic method.

2.2.1 Precursors

Analytical reagent grade reactants PbO (98%, Himedia), Bi_2O_3 (99.5%, Sigma Aldrich), TiO_2 (99 % Himedia), NiO (99.5%, Himedia), Nb_2O_5 (99.9%, Sigma Aldrich), Co_2O_3 (99 % Himedia), $BaCO_3$ (99 % Himedia), and K_2CO_3 (99.5 % Himedia) were used as the starting raw powders for preparation of samples. The reactants were characterized for phase purity by X-Ray Diffraction before using them. Prior to weigh the reactants, they were initially heated at 100^{o}C to remove the moisture.

2.2.2 Mixing and Milling

Stoichiometric amount of constituent reactants, required as per the nominal commission of a particular solid solution were first hand mixed in an agate mortar-pestle with AR grade acetone as the mixing medium. This mixture was transferred to a zirconia mixing jar which uses zirconia balls of 10 mm as the milling medium. The

ball-to-powder ratio was kept as 2:1 by weight. Now, AR grade acetone was added to the powder reactant mixture in jar and then ball-milled for 6 hours at 300 rpm by using planetary ball mill (Retsch, Germany).

2.2.3 Calcinations

The Ball Milled mixtures were dried at room temperature so that acetone gets evaporated. After drying the mixtures, dried powders were placed inside alumina crucibles for calcination. The calcination process was carried out using a Globar furnace. The calcinations time and temperature of a particular solid solution composition were optimized by calcining reactant mixture powder at different temperatures and time durations. For example, in $xPbTiO_3$-$(1-x)Bi(Ni_{2/3}Nb_{1/3})O_3$ solid solution, we have initially selected $0.65PbTiO_3$-$0.35Bi(Ni_{2/3}Nb_{1/3})O_3$(0.65PT-0.35BNNO) composition for calcinations at different temperatures ranging from 600^{o}C to 1000^{o}C. After grinding the calcined powder, x-ray diffraction patterns were recorded on fine powders. Fig. 2.2 shows the XRD patterns of 0.65PT-0.35BNNO powders obtained after calcination at different temperatures for 6.5 hours duration. XRD peaks corresponding to the perovskite phase are marked with “P”. The XRD peaks corresponding to the impurity/intermediate phases are marked with an asterisk (*). As can be seen from Fig.2.2, 0.65PT-0.35BNNO samples calcined at 600°C and 700°C reveal small peaks at $2\theta = 27.5°$ and $2\theta = 31.5°$ from non-perovskite phase. A very low intensity peak at $2\theta = 27.5°$ may be ascribed to the small amount of unreacted TiO_2 phase. The peak at $2\theta = 31.5°$ may be related to the secondary $Bi_4Ti_3O_{12}$ phase or a pyrochlore $PbTi_3O_7$ phase. The strong (110) perovskite peak present around 31.7°. Indicates the formation of perovskite phase at all the calcination temperatures.

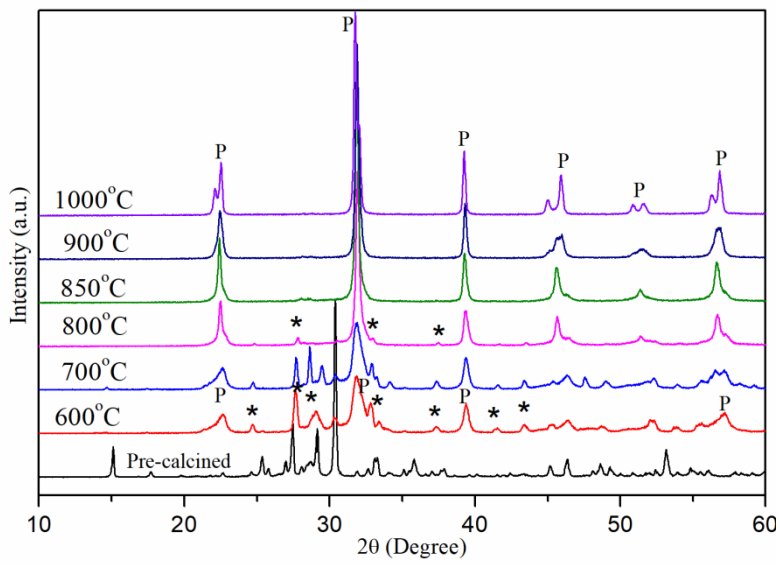

Figure 2.2 The XRD patterns of $0.65PbTiO_3$-$0.35Bi(Ni_{2/3}Nb_{1/3})O_3$ powders obtained after calcination at different temperatures for 6.5 hours duration. XRD peaks corresponding to perovskite phase are marked with "P" and intermediate/secondary phase peaks are marked with asterisk (*).

With increasing the calcination temperature from 600°C to 800°C, intensities of the impurity peaks decrease while perovskite peaks become more prominent. As shown in Fig. 2.2, for the samples calcined at 850°C temperature, no impurity peaks are observed in the XRD pattern. The XRD analysis of this sample also reveals good crystallinity of the pure perovskite phase. The absence of impurity for samples calcined at 850°C temperature indicates that 850°C is high enough optimum temperature to get phase pure samples. Notably, the splitting of the doublet characteristics of the tetragonal structure is clearly observed for sample calcined above 950°C, as shown in Fig.2.2.

As depicted in Fig. 2.2, the XRD peaks become sharp with increasing the calcinations temperature of samples that can be associated with the increased grain size of samples. Figs. 2.3 (a), (b) and (c) shows the SEM images of as synthesized polycrystalline $0.65PbTiO_3$-$0.35Bi(Ni_{2/3}Nb_{1/3})O_3$ ceramic samples calcined at 700°C,

850°C and 900°C, respectively. The corresponding EDS spectra are shown in the right panel of Figs. 2.3 (b), (d), (f) respectively. The EDS spectra confirm the presence of elements as per the composition. The SEM images shown in Fig. 2.3, confirm the increased grain size of the samples with increasing the calcination temperature. It is observed that 0.65PT-0.35BNNO ceramic calcined at 600°C consists of smaller sized grains (48 nm- 118 nm) while the sample calcined at 850°C shows bigger grain sizes ranging from 205 nm- 370 nm. The average particle size increases from 65 nm to 373 nm with increasing the calcination temperature of 0.65PT-0.35BNNO from 600°C to 850°C. The calcined powder particles are non-uniform and irregular in shape and size. Fig. 2.4 shows the XRD patterns of 0.65PT-0.35BNNO reactant mixture powder calcined at 850°C with varying the calcination time (2h, 6.5h, 14h and 24 h). Sample calcined only for 2 hours shows small impurity peaks. When the calcination time is increased to 6.5 hours, impurities are removed. On further increasing the calcinations time by more than 14 hours, the impurities are resurfaced in XRD patterns that can be attributed to the loss of volatile Bi_2O_3 or PbO. Therefore, we have chosen optimum calcination temperature as 850°C and optimum calcination time as 6.5 h for ceramics sample preparation.

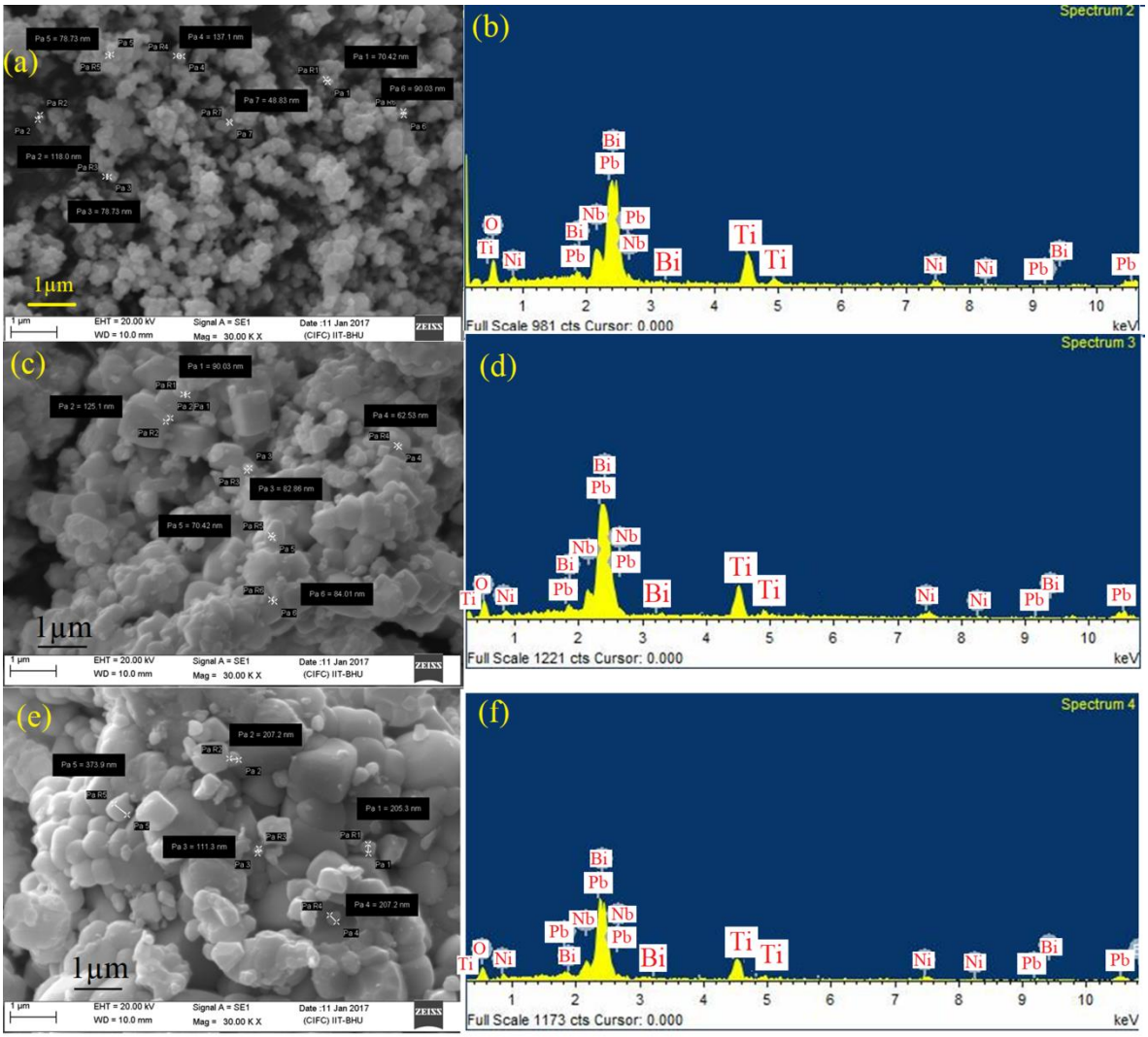

Figure 2.3 SEM images of as synthesized polycrystalline $0.65PbTiO_3$-$0.35Bi(Ni_{2/3}Nb_{1/3})O_3$ ceramic calcined at (a) 700°C (c) 850°C (e) 900°C and corresponding EDS spectra in the right panel (b), (d), (f) respectively, showing the presence of elements as per the composition.

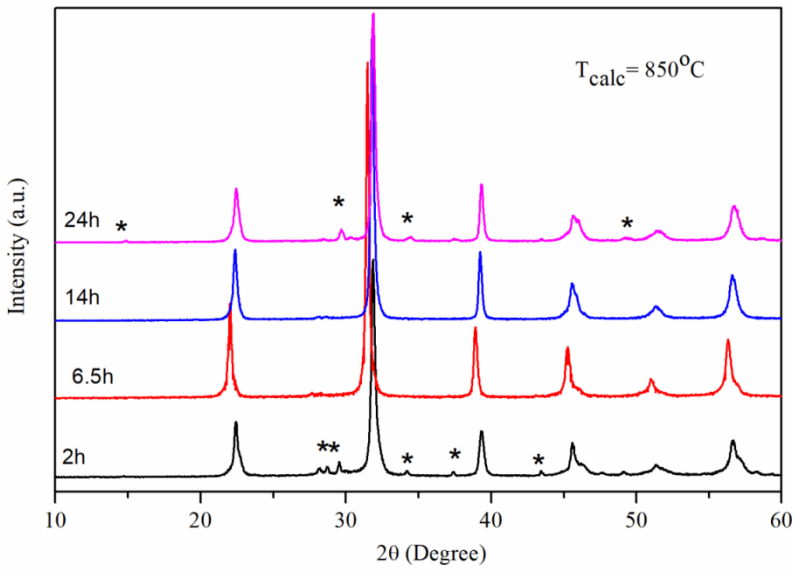

Figure 2.4 The XRD patterns of $0.65PbTiO_3$-$0.35Bi(Ni_{2/3}Nb_{1/3})O_3$ powders obtained after calcination at 850°C temperature with varying the calcination time duration.

2.2.4 Preparation of Green Pellets and Target

The calcined mixture was crushed and then ball milled for 2h to remove any agglomerates. Before preparing the green pellets, an organic binder was mixed with obtained fine powder. We have used an organic binder of 2% polyvinyl alcohol (PVA) in water solution. The homogeneous mixture of PVA solution binder and calcined powder was used for the preparation of green pellets. Green pellets of ceramic samples were made with the help of cylindrical stainless steel die of 12 mm diameter. PVA binder mixed powder was kept in die and uniaxially pressed by a hydraulic press. We have also optimized the load pressure to prepare good quality green pellets so that a high-density pellet can be prepared after sintering. We have obtained an optimized load of 65kN, and this load was used to prepare the pellets. A similar procedure was adopted for preparation of 2-inch diameter PLD, and sputtering target pellets. The Cold compaction of mixture was done using larger diameter 55 mm cylindrical steel die.

2.2.5 Sintering

The dielectric and ferroelectric properties of ceramics strongly depend on the density of the compact pellets, so the green pellets were sintered at optimized sintering temperature and time duration. The sintering process requires green pellets without any organic binder. So, before sintering, it is necessary to remove the polymer binder from the green pellets. Annealing process of the green pellets at 500°C results in evaporation of PVA organic binder. Due to the volatile nature of Bi and Pb-oxides at higher temperatures, the sintering process was performed inside a closed and properly sealed alumina crucible. To prevent and compensate the Bi and Pb loss during sintering process, we have kept small quantity of calcined powder of same composition inside the crucible along with the green pellets. The sintering temperature and density of pellets were optimized to ensure minimum weight loss (<0.5%). Fig. 2.5 shows the XRD patterns of 0.65PT-0.35BNNO composition sintered at various temperatures and time duration. It is observed that longer sintering time duration at 1090°C causes creation of additional impure phases which may be due to Bi and Pb loss. The optimized sintering temperature and sintering duration were found to be 1090°C and 1 h respectively. Archimedes principle was used to calculate the density of the sintered pellets. Densities of the sintered pellets were greater than 96% of the theoretical density. To collect the XRD data, the sintered pellet was crushed into fine powders and annealed at 500°C for 10 hours to eliminate possible strains in samples. These strains may develop during the process of crushing, so, it is necessary to remove them. The annealed sample was used for acquiring the XRD data. The XRD patterns of one representative solid solution system xPT-(1-x)BNNO with compositions x = 0.87, 0.77, 0.70, 0.67, 0.66, 0.65, 0.64, 0.63, 0.60, 0.55 and 0.50 are shown in Fig. 2.6. The compositions with lower PT concentrations have negligibly weak impurity peaks around 29^{o} two theta angle which

is attributed to less stability of perovskite phase for BNNO component as is known for many other Bi-based perovskites [R. Rai et al. (2009); R. Pandey et al. (2013); A. Upadhyay et al. (2015);].

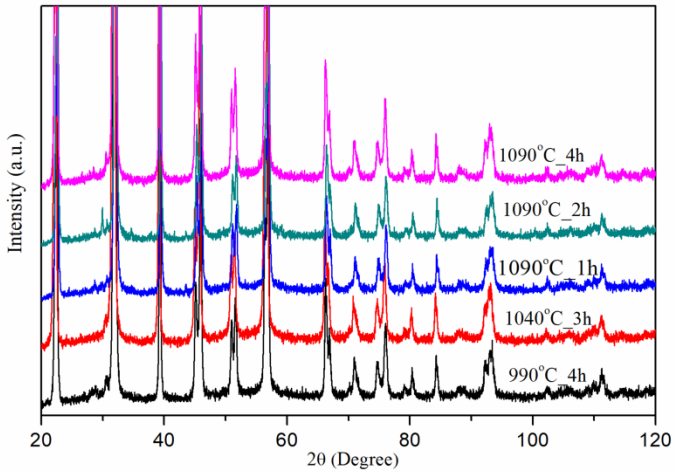

Figure 2.5 XRD patterns of sintered 0.65PT-0.35BNNO samples with varying the sintering temperature and time.

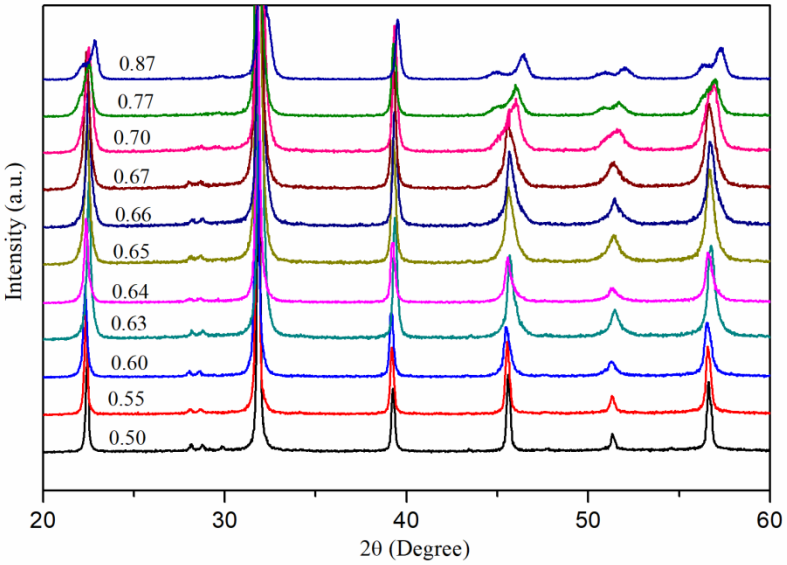

Figure 2.6 XRD patterns of xPT-(1-x)BNNO sintered samples with compositions x = 0.87, 0.77, 0.70, 0.67, 0.66, 0.65, 0.64, 0.63, 0.60, 0.55 and 0.50.

2.3 Microstructural and Compositional Study

The microstructural studies of sintered ceramic samples for different compositions of investigated solid solutions were conducted using the Scanning

electron microscopy (SEM). The compositional analysis was done on the sintered pellets with surfaces energy dispersive X-ray spectroscopy (EDS) technique. SEM measurement was performed using high-resolution scanning electron microscope (HR-SEM) (Nova NanoSEM 450, FEI) equipped with energy-dispersive X-ray spectroscopy (EDS) measurement attachment. Fig. 2.7 depicts the SEM images of a representative 0.65PT-0.35BNNO compositions sintered at 990°C, 1040°C and 1090°C. It is observed that the grain size and microstructure of PT-BNNO ceramics are affected by the sintering temperature. With increasing the sintering temperature, the grain size and densification increases as can be observed from Fig. 2.7 (a), (b) and (c) insets. For sample sintered at 990°C, grain size is in the range of 300 nm- 900 nm while for 1090°C sintered sample grain size increases in the range 950 nm – 3.5 μm. The SEM images reveal that with increasing the sintering temperature, the grain size increases and non-uniformity in grain size also increases.

The energy dispersive X-ray spectra (EDS) maps for 0.65PT-0.35BNNO composition are shown in Fig. 2.7(a-c). The EDS investigation confirms the presence of Pb, Ti, Ni, Nb, Bi, and O elements. There is no other impurity element found. In EDS, the characteristic peaks of all the constituent elements without any impurity confirm the pure composition of the synthesized solid solution. Fig. 2.8 shows the elemental mapping of 0.77PT-0.23BNNO. Elemental mapping of sample confirms well the homogeneous distribution of Pb, Ti, Ni, Nb, Bi, and O elements according to their doping percentage.

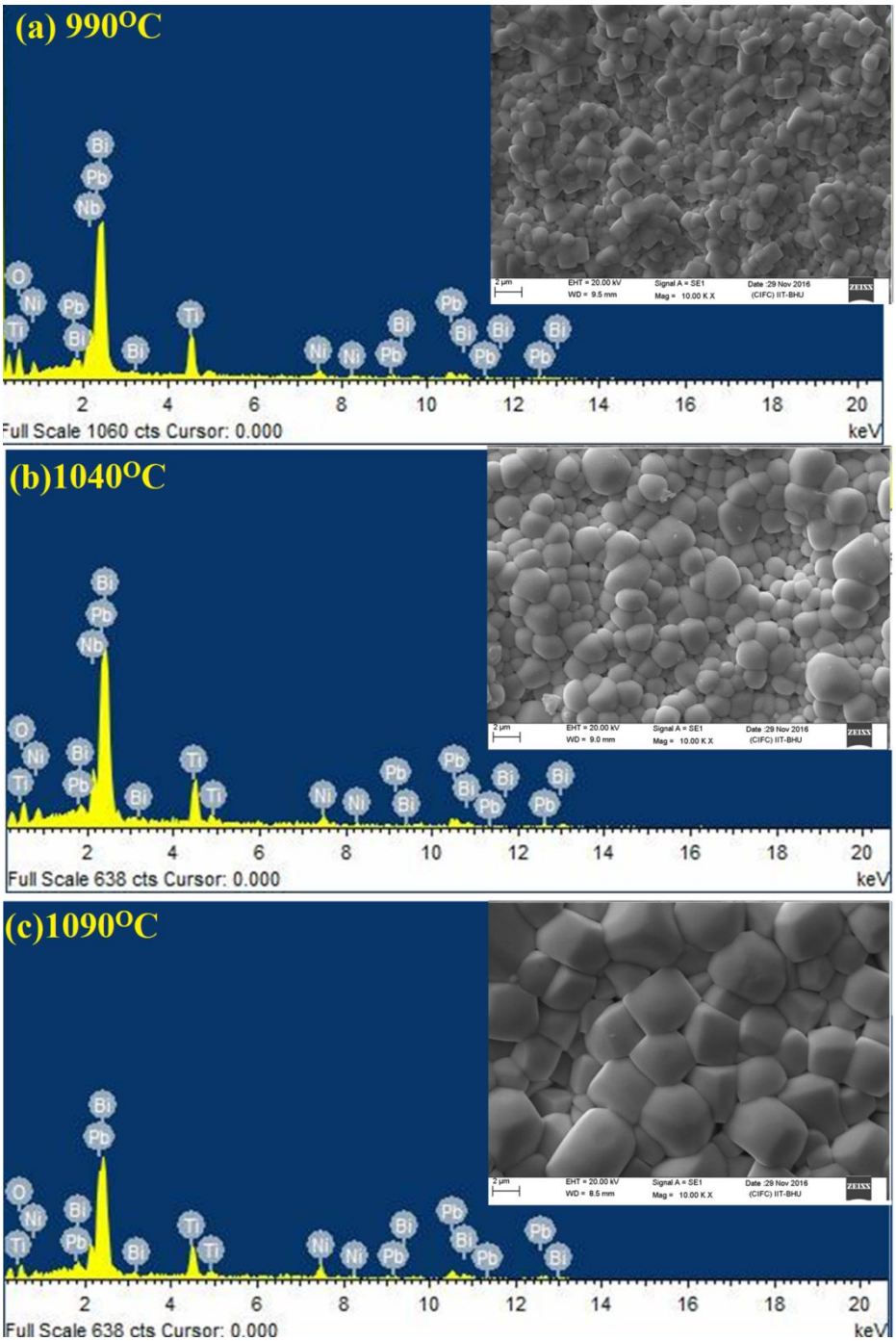

Figure 2.7 Scanning electron micrographs and EDX spectra of 0.65PT-0.35BNNO samples sintered at (a) 990°C, (b) 1040°C and (c) 1090°C.

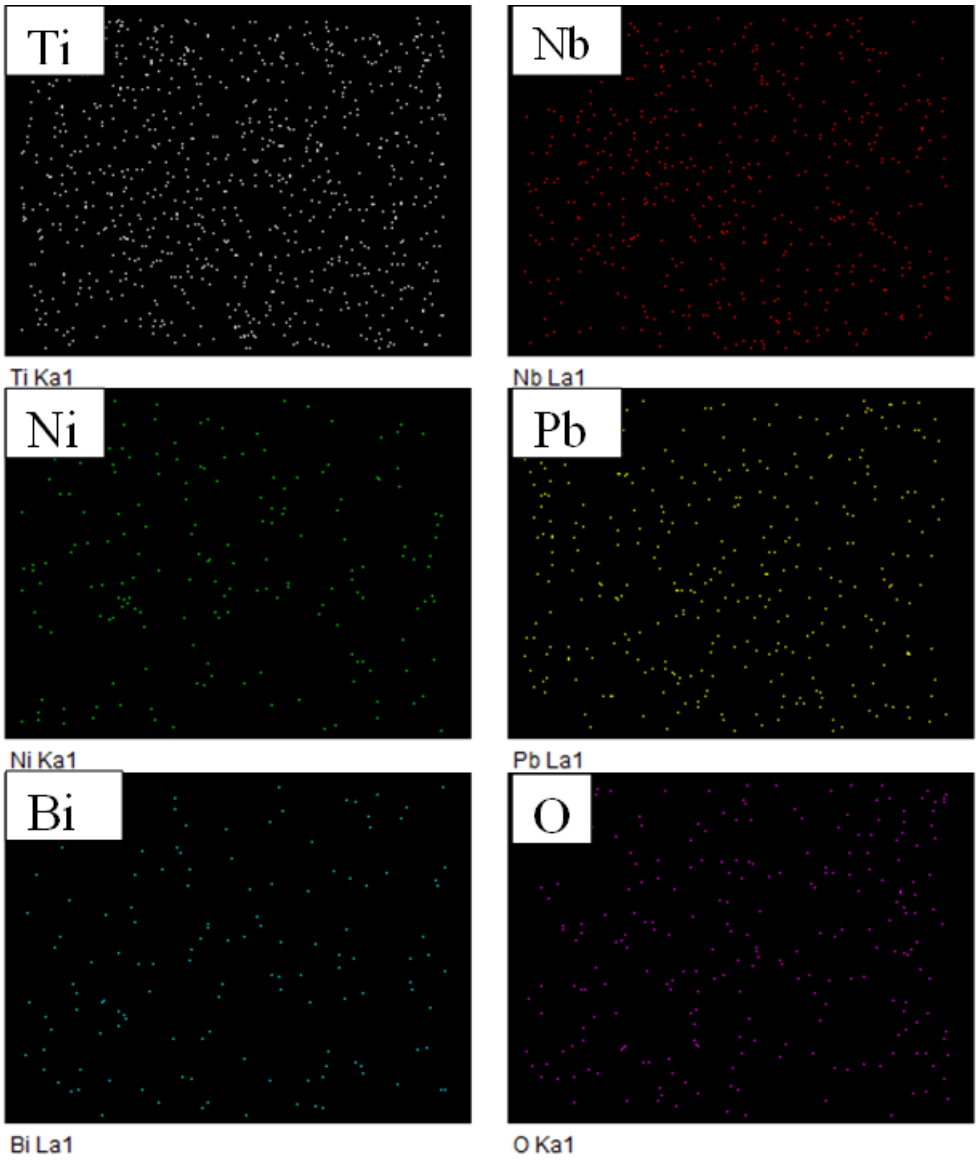

Figure 2.8 Elemental mapping of sintered 0.77PT-0.23BNNO solid solution.

2.4 Preparation of Ferroelectric thin film samples

Ferroelectric materials are the future of thin film technology for photovoltaic, dielectric, ferroelectric etc. applications. New advanced deposition techniques are being used to deposit ferroelectric thin films to precisely control the composition, microstructure and physical properties. Ferroelectric materials have several advantages over other photovoltaic materials including low cost, high open circuit photo voltage, switchable diode effect etc. In existing literature, different approaches have been used

to grow ferroelectric thin films such as pulsed laser deposition (PLD), magnetron sputtering and chemical solution deposition (CSD). In following sections, deposition methods that were used in this work are described.

2.4.1 Pulsed laser deposition (PLD)

The advantage of PLD over other deposition methods for ferroelectric thin film is that grown films have more possibility to contain the same composition identical to that of a target. PLD is a type of physical vapour deposition in which a high powered pulsed laser beam is focused to strike a solid material (target). The short pulse of high energy laser provides so great thermal spike on the target that all of its components get evaporated while maintaining their stoichiometric composition. The evaporated sample is deposited on a suitable placed substrate of desired characteristics. In this method, the obtained film's thickness and physical properties depend on the laser fluence, pulse duration, wavelength, laser spot size and target-to-substrate distance [Ed. H. S. Nalwa (2002)]. The thin film growth by the PLD involves various steps such as laser irradiation on target, rapid heating of target and vaporization of material, formation of plasma which contains neutral atoms, molecules and ions, as well as energetic electrons. The final stage of PLD process is nucleation and growth of thin film on the substrate [Ref. D. H. Lowndes et al. (1996)]. The nucleation and growth of film depend on type of substrate, deposition temperature, and energy. In the PLD process, ultra-thin and smooth films can be obtained due to the short laser pulsed duration and layer-by-layer nucleation. A typical setup and schematic illustration for PLD deposition process is shown in Fig.2.9 and Fig. 2.10. It uses ultra-high vacuum chamber, KrF excimer laser source, and mechanical and turbo molecular pump. The target is struck at an angle of 45 from a pulsed and focused laser beam.

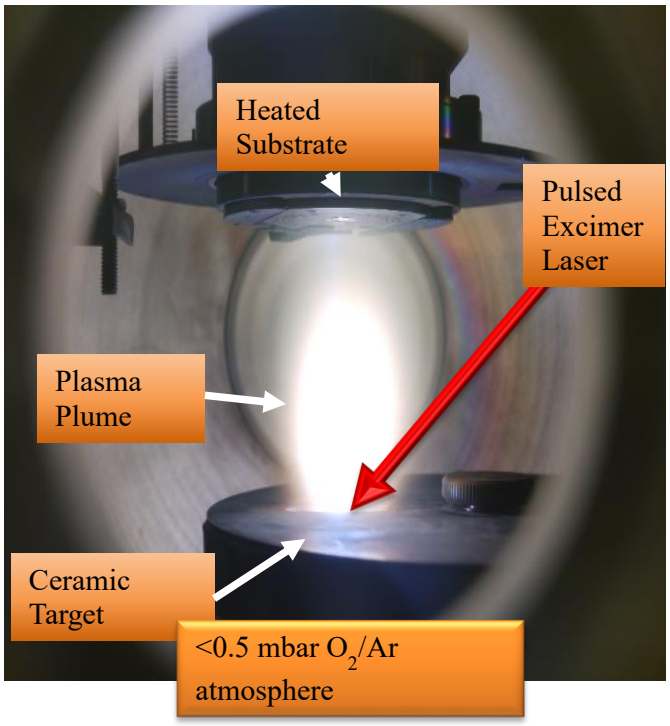

Figure 2.9 Image of a Pulsed laser deposition chamber unit during its operation.

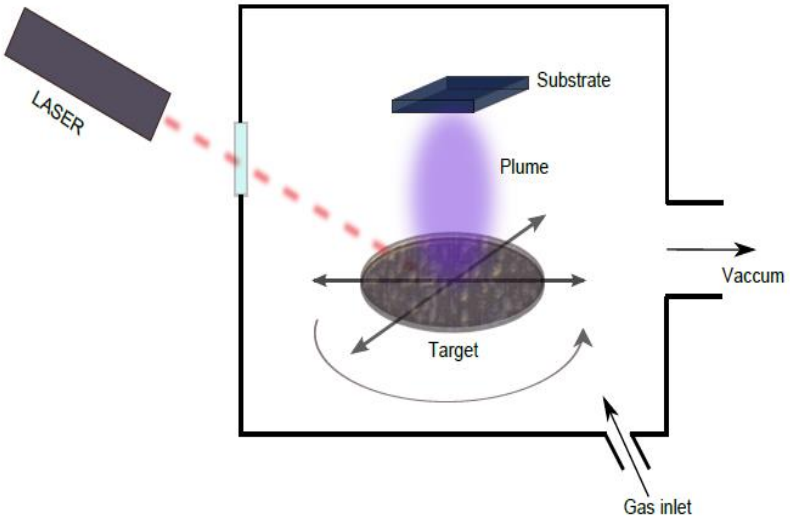

.

Figure 2.10 Schematic diagram of Pulsed laser deposition unit.

2.4.2 RF Magnetron Sputtering

Magnetron sputtering deposition method is extensively used procedure to grow thin films in bigger dimensions and large quantity. The sputtering process is based on

ion bombardment on a source material that acts as a target. DC (direct current) sputtering technique is usually applicable for conductive targets only, while RF (radio frequency) sputtering is applicable for targets that are conductive as well non-conductive in nature. During the sputtering process, energetic particles from plasma strike on the target, and due to this bombardment of the ions and charged particles, several atoms/molecules are ejected from the target. There are two methods to generate the energetic particles for sputtering ion beam and plasma. In plasma-based sputtering, the target is connected to the cathode, and a high negative voltage is applied to the cathode. The positively charged ions from the plasma are attracted by the cathode and bombard target to start the sputtering process. Fig. 2.11 shows the schematic diagram of a sputtering unit and the sputtering process. The target and substrate holder are in the opposite directions, and the substrate holder is in anode condition.

The chamber is evacuated to its base pressure 10^{-6} mbar before introducing the Ar/O_2 gases. Partial gas pressure is maintained to create the plasma. When a high voltage difference is created between the cathode and anode, a glow discharge is ignited [Ed. P. M. Martin (2010)]. To sustain the glow discharge with the insulator target, the RF-power supply is used. The RF-sputtering unit uses an impedance-matching network between power supply and discharge chamber. Being non-conductive insulating or semiconducting in nature, various ferroelectric thin films were successfully deposited by RF magnetron sputtering [A. Iljinas et al. (2015)]. Good quality $BiFeO_3$ thin films were also deposited by RF-magnetron sputtering method [J. Wu et al. (2010)].

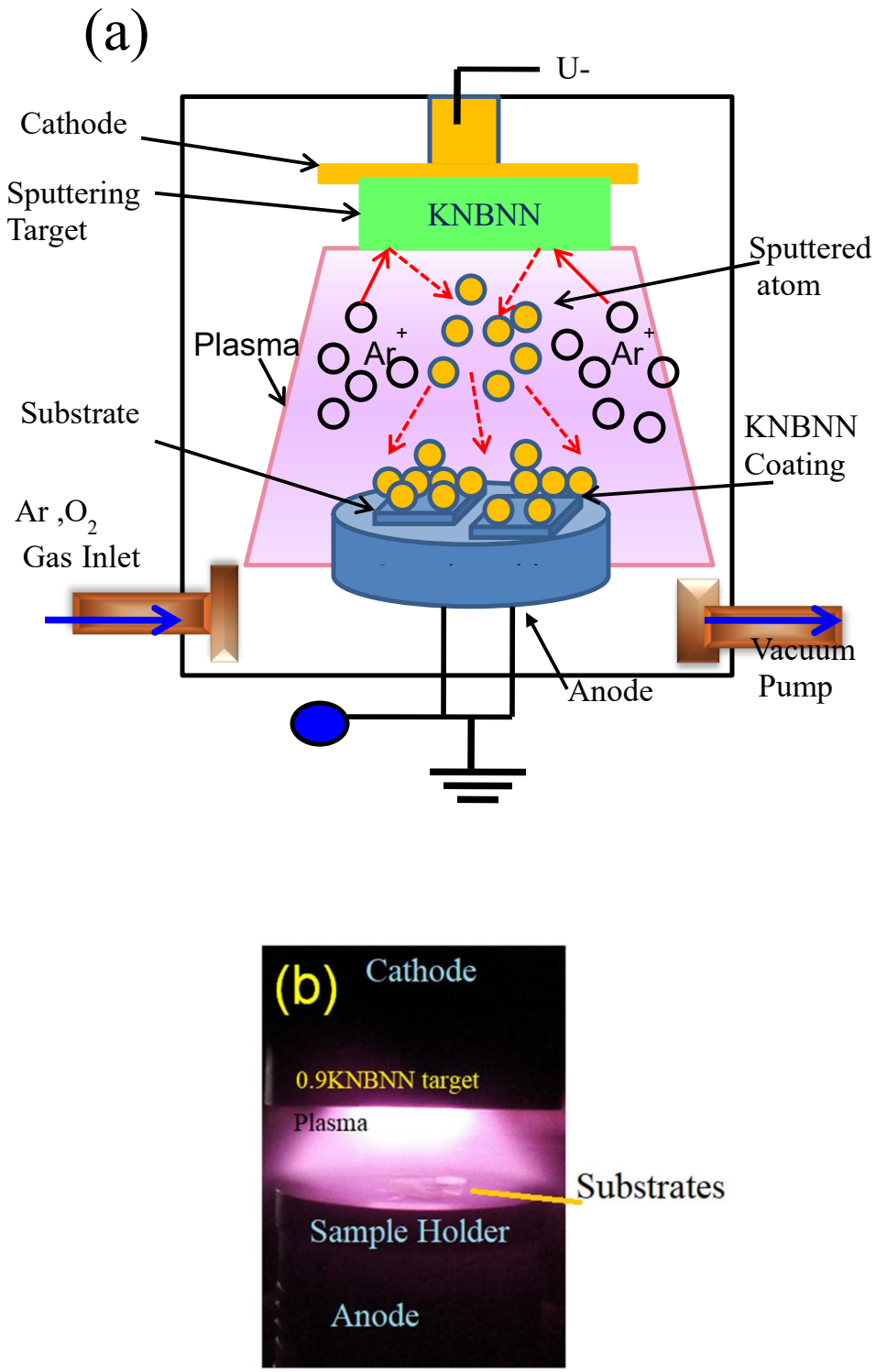

Figure 2.11 (a) Illustration of magnetron sputtering system and process (b) Image of a rf-magnetron sputtering unit during its operation.

2.4.3 Sol-gel based deposition technique

The chemical solution deposition (CSD) usually by spin coating process is used to achieve better composition control in multi-component systems for large area coating and low-cost methods. The $PbTiO_3$ and $Pb(Zr, Ti)O_3$ thin films were successfully deposited by CSD method [S. K. Dey et al. (1988)]. The CSD method has been widely used to grow PZT thin films for their applications in capacitors, electro-optic devices, sensors, and surface acoustic devices. The $BiFeO_3$ thin films were successfully grown on ITO and FTO substrate by CSD method [X. Chen et al. (2012)]. The CSD method consists of following steps: precursor solution preparation, spin coating of precursor solution on the substrate, drying of the film at 100°C, pyrolysis of organic species at 300°C -500°C, crystallization and densification of the films at (550 °C -750 °C) to get perovskite phase. Fig. 2.13 shows the various steps of thin film deposition by CSD method. The thin films are spin-coated on a substrate and first dried at 100°C to remove the solvent from the film. Subsequently, the sample is annealed at 350°C to remove its organics species component. For crystallization and densification, films were annealed at 550°C to 750°C using rapid thermal annealing. During crystallization process, first the films which are in amorphous phase are converted into oxygen-deficient pyrochlore phases when temperature is more than 500°C. The thin films start crystallizing at temperatures above 500°C. The transformation of thin films from amorphous to the perovskite phase starts above 700°C, and it also depends on annealing time and solution chemistry [S. K. Dey et al. (1988)]. Fig 2.12(a) illustrate the schematic diagram of spin coating process, and (b) shows the effect of annealing temperature on spin-coated films. Fig. 2.13 shows the schematic diagram of CSD spin coating method used to grow the $(1-x)KNbO_3$-$xBa(Ni_{1/2}Nb_{1/2})O_3$ thin films in present thesis.

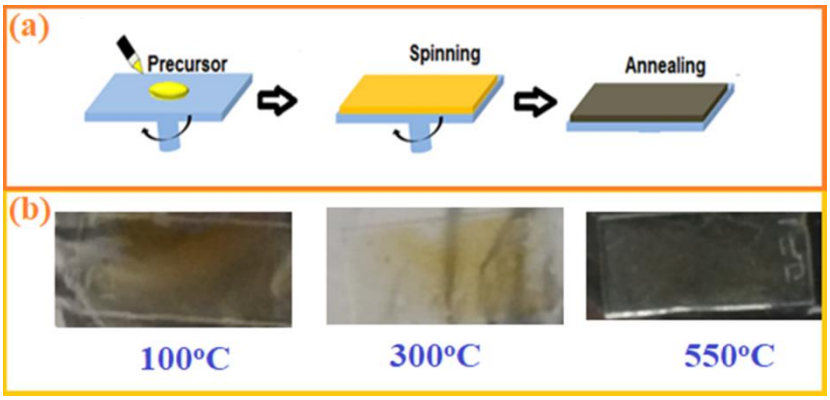

Figure 2.12 (a) Schematic illustrations of spin coating process and (b) effect of annealing temperature on spin coated films.

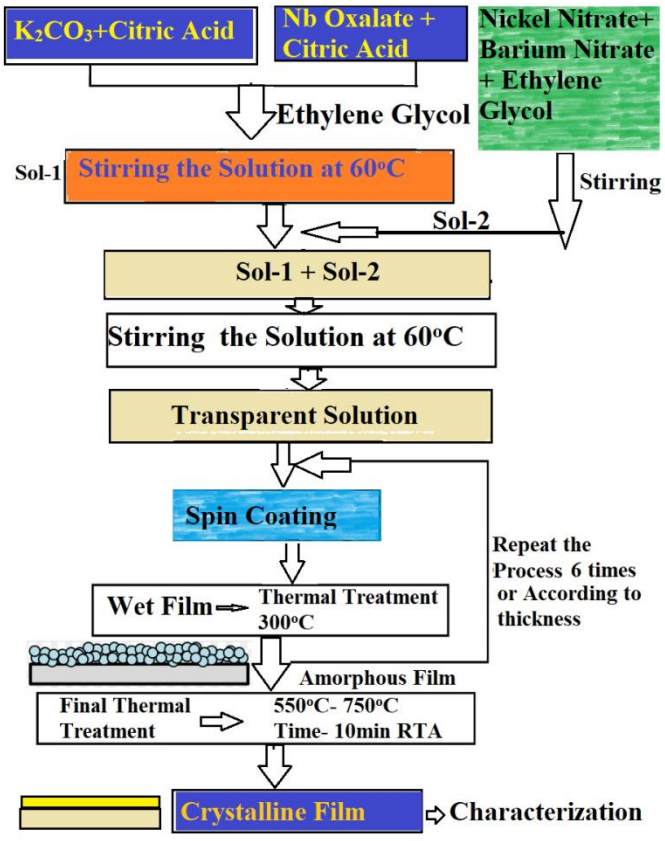

Fig. 2.13 Schematic illustrations of thin film deposition steps by chemical solution deposition technique for (1-x)$KNbO_3$-x$Ba(Ni_{1/2}Nb_{1/2})O_3$ ceramic.

2.5 Device fabrication process

2.5.1 Substrate Cleaning

For thin film deposition and ferroelectric photovoltaic device fabrication, quartz, silicon wafer, and FTO coated glass substrates (surface resistivity ~ 8Ω/sq) were used in the present thesis work. Before any deposition, it is necessary to clean the substrates to remove any surface impurity. The substrates may contain various contaminants such as dust particles, oils from human hands during cutting. For dust particles removal, simple water cleaning is required. So, substrates were first cleaned by soap solution by using a brush. After cleaning with normal water, the substrates were cleaned by de-ionized water. The substrates were then rinsed in acetone and ultrasonic cleaning was done for 15 min. Again, the substrates were cleaned with de-ionized water and then rinsed in ethyl alcohol to remove ultrafine particles and moisture. Quartz and silicon substrates were cleaned with a mixed solution of de-ionized water, Hydrogen peroxide and ammonia. The substrates were placed in this solution for 15 min at 80^{o}C. After further cleaning with de-ionized water and ethyl alcohol, the substrates were dried at 100 ^{o}C in the oven.

2.5.2 Processing steps for device fabrication

A Schematic illustration of various fabrication process steps of ZnO:Al/x$BaTiO_3$-(1-x)$Bi(Ni_{2/3}Nb_{1/3})O_3$/Ag (AZO/BT-BNN/Ag) heterojunction device mounted on Si wafer is shown in Fig. 2.14. The thin BT-BNN pellet is sandwiched between two electrodes. Fig 2.14 depicts the representative device configuration during I-V measurement with AZO/BT-BNN/Ag where Ag acts as the bottom electrode and AZO acts as the top electrode. The ferroelectric ceramics were polished to a thickness of ~ 600 μm and mounted on a silicon wafer with silver epoxy. This silver epoxy served

as the bottom electrode after drying at 500°C. For the top electrode, thin film of ZnO:Al (AZO) is deposited on BT-BNN surface by magnetron sputtering. The circular top electrode is fabricated on BT-BNN surface using a patterned shadow mask and at 200°C substrate temperature for better adhesion of the film. The thickness of AZO layer is determined to be ~ 150 nm with a resistance of less than 200 Ω. The ferroelectric pellet device was poled before I-V measurements at 100°C for 30 minutes. The poling voltage was decided according to the thickness of pellet and coercive field of BT-BNN composition.

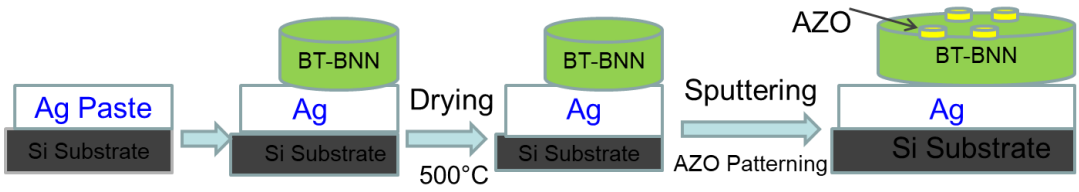

Figure 2.14 Schematic illustrations of device Fabrication steps on Si substrate using silver paste and thin ferroelectric pellet.

Thin film based photovoltaic device fabrication process is illustrated in Fig. 2.15. First Ferroelectric thin film was grown on FTO coated substrate and MoO_3 film deposited as hole transport layer. Ag deposited on top of this layer acts as conducting electrode. The thickness of Ag electrode was around 100 nm. A schematic representation of the photovoltaic device is shown in Fig. 2.16, where a platinum tip of AFM is used to measure the I-V curve. Schematic illustration of device architecture on FTO glass substrate using MoO_3 as hole transport layer and ZnO as electron transport layer with ferroelectric layer as active photovoltaic material is shown in Fig. 2.17.

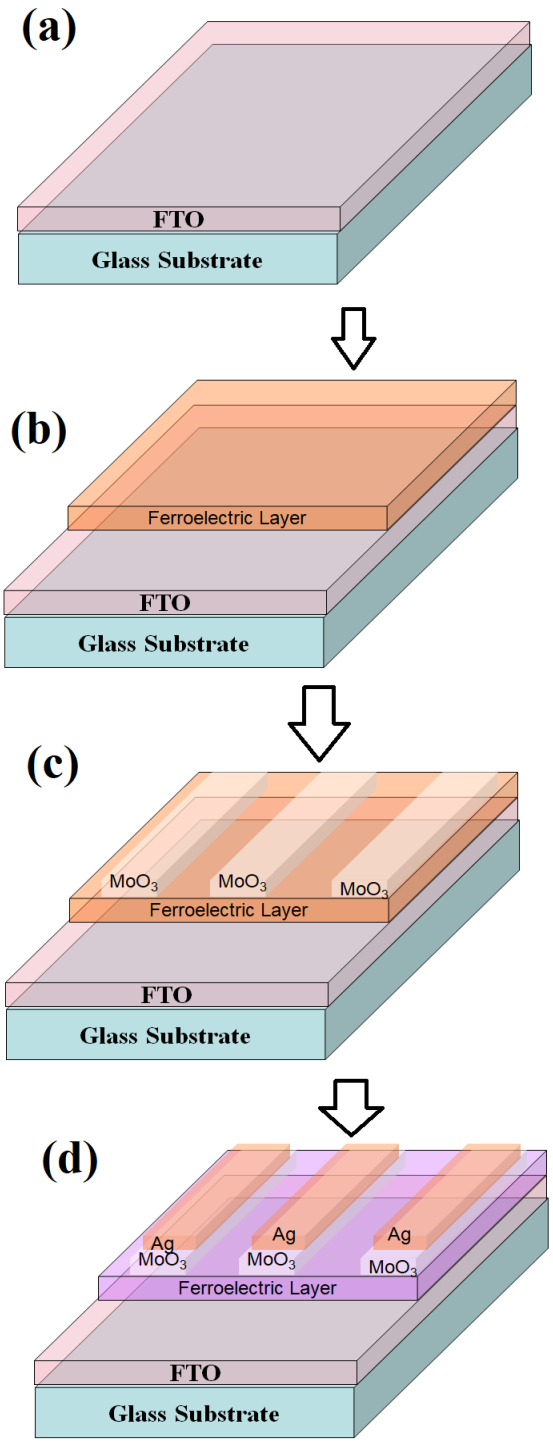

Figure 2.15 Schematic illustration of device Fabrication steps on FTO glass substrate.

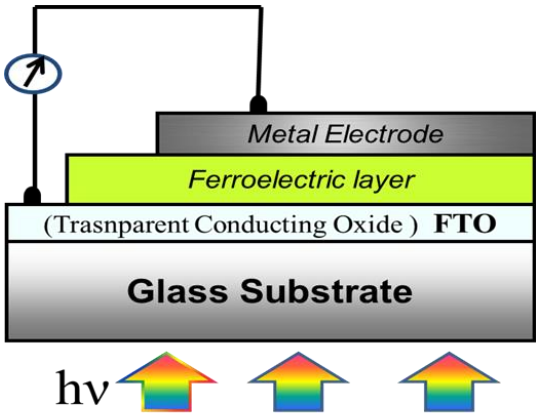

Figure 2.16 Sketch of bottom-top electrodes configuration for ferroelectric films.

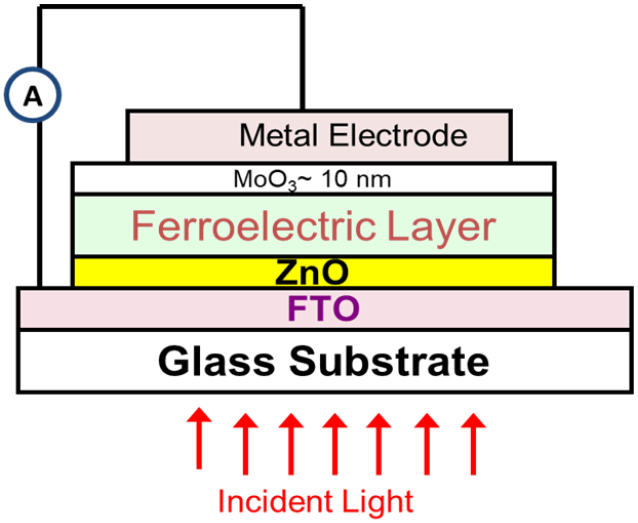

Figure 2.17 Schematic illustration of device architecture on FTO glass substrate using MoO_3 as hole transport layer and ZnO as electron transport layer with ferroelectric layer.

2.5.3 Electrode deposition

The metal electrodes were deposited by physical vapour deposition (PVD). The source metal is heated to its boiling temperature in vacuum environment. The escaping vapour atoms travel in a straight line and collide with substrate and chamber wall. When vapour species (atoms/molecules) reaches on a substrate, condensation starts, and after nucleation, thin film grows. In this work, Au, Ag and MoO_3 were deposited by

PVD. The ZnO:Al (AZO) thin films were also used as top electrode in some photovoltaic devices investigated in the present thesis and it was deposited by pulsed DC magnetron sputtering. Fig. 2.18 (a) shows the XRD diffraction pattern of AZO thin film and Fig.2.18 (b) shows its percentage transmittance which is more than 80%. The atomic force microscopy image depicts its topography as shown in Fig 2.18 (c) and (d). As can be seen from these figures, the deposited AZO film is of good quality.

We have used $SrRuO_3$ also as the bottom electrode in some devices. The $SrRuO_3$ (SRO) thin films were grown on glass and FTO substrates by sol-gel based spin coating method. Perovskite oxide based conductive layers as electrodes have drawn enormous attention due to their physical and chemical stability at high temperatures. These conductive perovskite oxides also have the advantage to help in growth of ferroelectric films on their surface due to a similar lattice constant. Solution processed SRO thin films were successfully synthesized by optimizing various preparation conditions. $SrCl_2$ and $RuCl_2.xH_2O$ were dissolved in 2-methoxyethanol at 1:1 molar ratio to produce a mixed SRO precursor solution. SRO films were deposited on quartz and silicon substrates by spin coating method. SRO films with various thicknesses were prepared by controlling the spin speed and deposition time. All films were first dried at 350^{o}C and sintered at 600–800 ^{o}C to get crystalline and phase pure structure. The growth rates of solution-processed films depend on drying conditions. Fig. 2.19 demonstrates the AFM Topography image of $SrRuO_3$ (SRO) thin films deposited in different layers viz. (a) single layer (b) 3 layers (c) 6 layers, with their corresponding 3-D images in (d), (e), (f) and roughness profiles in (g), (h), (i), respectively. The XRD patterns of single layer SRO films with different spinning speed are shown in Fig. 2.19 (j) and for 6-layer films in Fig. 2.19 (k). The variation of resistivity of SRO films with varying number of layers is shown in Fig.2.19 (l). The electrical resistivity of SRO thin

films was around 10 $^{-2}$ Ohm-cm range, which is less than resistivity of the single crystal SRO ($3x10^{-4}$ Ohm-cm) as shown in Fig.2.19 (l). As the number of layers increases the resistivity decreases. SRO films show high metallic conductivity and high temperature stability in an oxidizing atmosphere.

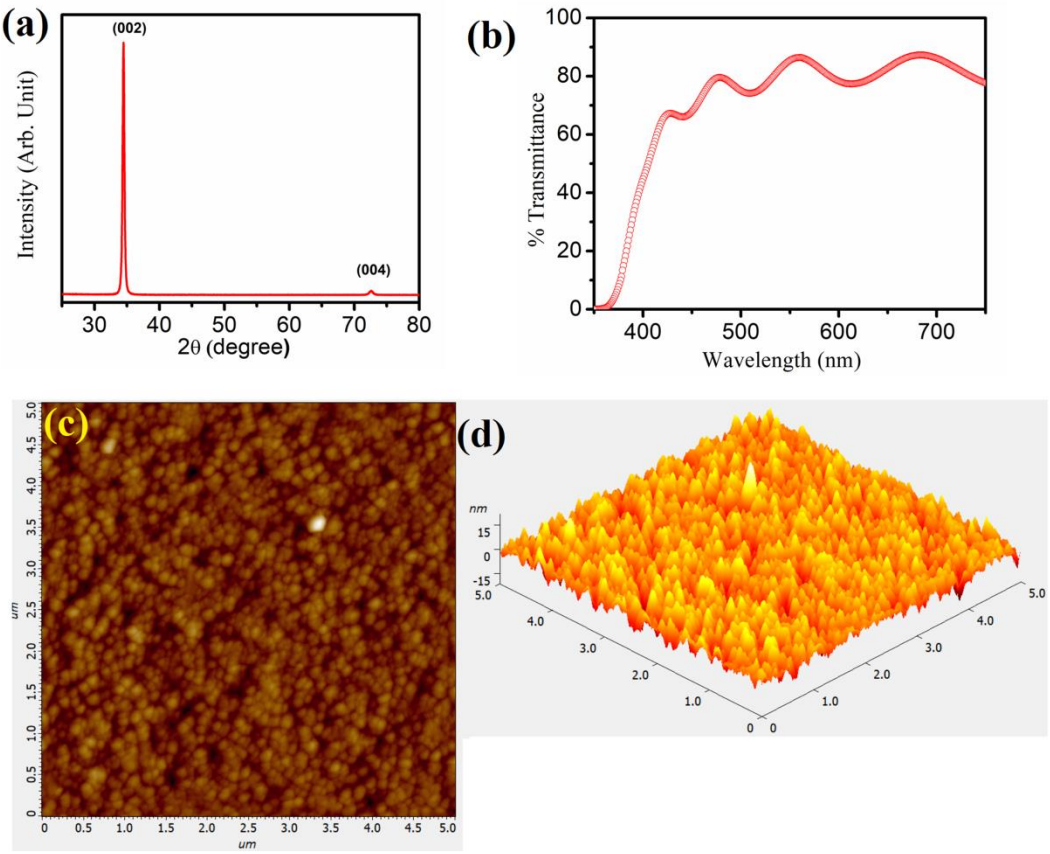

Figure 2.18 (a) XRD pattern (b) Transmittance (c) AFM topography image and (d) 3-D image of AZO thin film.

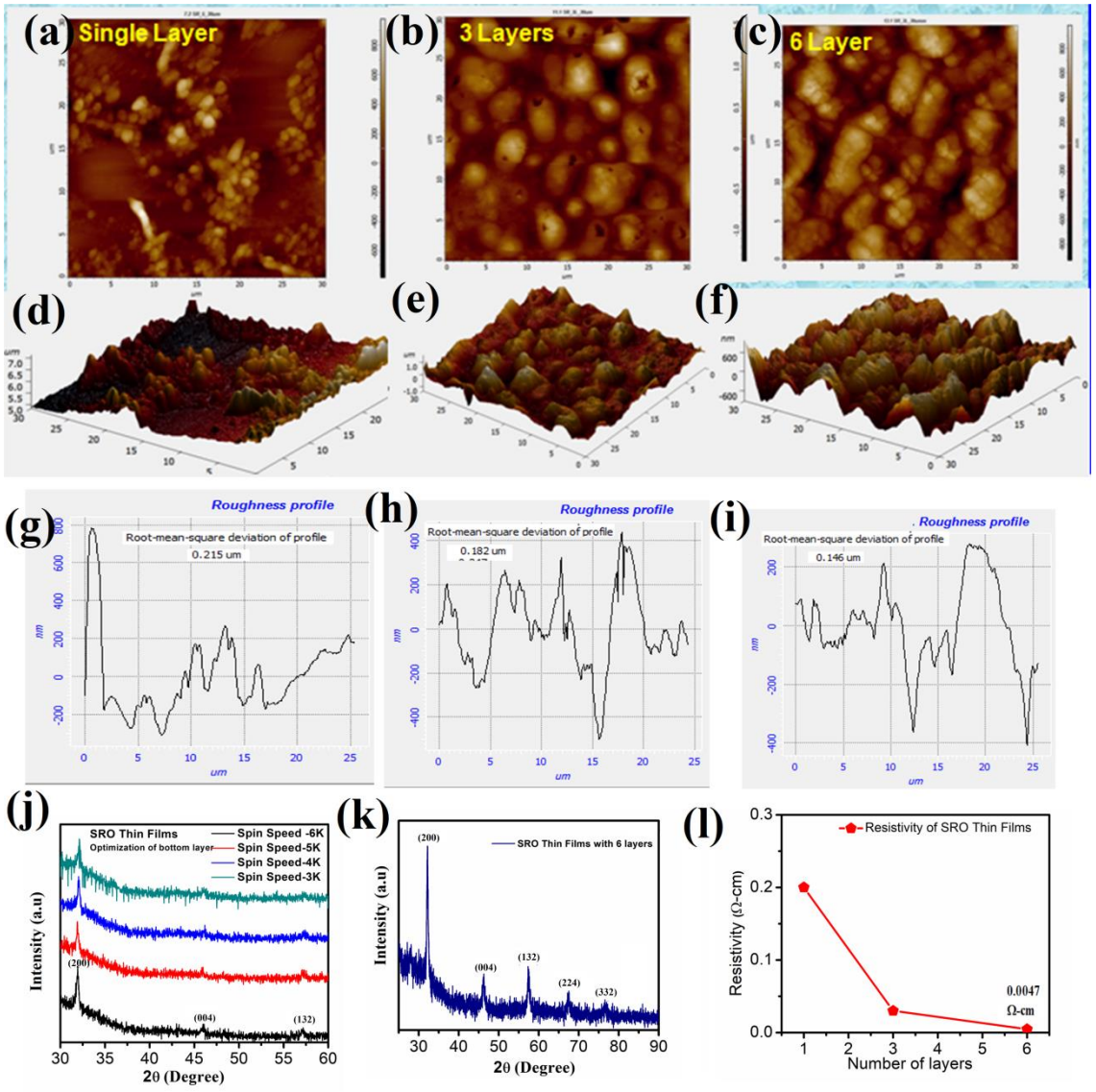

Figure 2.19 AFM Topography image of $SrRuO_3$ (SRO) thin film (a) single layer (b) 3 layers (c) 6 layers, (d), (e), (f) showing their 3-D image, (g), (h), (i) showing their roughness profile respectively. (j) XRD pattern of single layer SRO films (k) XRD pattern of 6 layers SRO film (l) resistivity of SRO films with varying number of layers.

2.6 Bulk ceramics and thin films characterization techniques

2.6.1 XRD

The powder X-ray diffraction (XRD) technique is a widely used tool to analyze the crystallographic phase and structural properties of materials. It is a non-invasive technique for analyzing the structural characteristics of all types of crystalline materials. XRD is used to identify phases in unknown materials, structural and phase purities in newly developed materials. The coherent parallel beam of incoming X-rays scatters from parallel planes of atoms within a crystal. The atomic spacing in crystals is in angstrom order, so X-rays are used to study crystalline structure as their wavelength is also of same order. When X-ray beam is incident on a specimen, coherent X-ray scattering is observed. The intensity and spatial distribution of the scattered X-Rays form a specific diffraction pattern is the 'fingerprint' of the specimen [Cullity (1978)]. The diffraction pattern and material's structure can be related by Bragg's law. The Bragg's law is expressed mathematically as $2d_{hkl} \sin \theta = n\lambda$, where '$d_{hkl}$' is the interplanar lattice spacing, 'θ' is the diffraction angle, 'λ' is the wavelength of the X-ray and 'n' is the order of diffraction. The diffraction angles corresponding to different peaks in the x-ray diffraction pattern are matched with a standard diffraction pattern (JCPDS/ICDD file) to know about the phase and crystal structure of the material. For unknown materials, diffraction pattern is indexed to determine the crystal system and lattice parameters. An XRD study has been used to characterize the crystalline phase of as prepared perovskite solid solutions. Powder XRD measurements were carried out at room temperature from 20^o to 120^o using a powder diffractometer (RIGAKU SmartLab and MINIFLEX 600) with Cu-K_α radiations. Crystal structure analysis was performed by Rietveld refinement using FULLPROF suite [J.R. Carvajal (1993)]. For thin films, grazing incidence X-ray diffraction (GIXRD) is used. Grazing incidence is a type of

diffraction geometry with incident angle very close to a critical angle of the film, and incident rays are diffracted almost in the plane of thin film.

2.6.2 Scanning Electron Microscopy

The microstructures of as-synthesized materials were investigated using a scanning electron microscope (ZEISS, Evo 18 Research). In a scanning electron microscope (SEM), a focused beam of electrons is used to scan the sample surface. The electrons incident on the sample surface interacts with the atoms in the material. The interaction of electrons with the surface produces secondary electrons (SE), backscattered electrons (BSE) and other types of signals, which are collected, amplified and detected with a scintillator-photomultiplier detector. The collected signals are converted into electrical signals and the scan is used to generate an image of the material's surface on a cathode ray tube display or computer display. The chemical composition of material, presence of elements and their concentration are analyzed through energy dispersive X-ray (EDS) spectrometer fitted with SEM. The advantage of the EDS is that the X-rays generated from a wide range of elements are analyzed simultaneously for the accurate compositional analysis. An X-ray spectrum in EDS enables us to execute a quantitative study about what elements are present in the specimen area irradiated by the electron beam. The function of an EDS spectroscopy is based on stimulating the materials with uniform energy through an electron beam. Each element in the investigated material generates X-ray of specific energies as per the energy difference of inner orbitals which help to identify the elements in the composition. The cross-section of thin films was imaged by high resolution SEM. The HRSEM used in this work is a Nova Nano SEM 450, FEI Company of USA (S.E.A.) PTE, LTD.

2.6.3 Transmission Electron Microscopy

The transmission electron microscopy (TEM) is another important characterization technique in which the materials are investigated by the signals generated due to interaction of transmitted electrons of a focused electron beam through the thin section of the material. Magnetic lenses are used to control and focus the electron beam generated from an electron gun that can be a tungsten filament or field emission (LaB_6) based. The entire microscope column and sample chamber works under high vacuum as the presence of gas molecules will scatter the electrons or a discharge can take place. The TEM has two modes of operation: the imaging mode and the diffraction mode. In imaging mode, the image of the sample is formed in the image plane of the objective which is then magnified by a series of projector lenses. In diffraction mode, the diffracted beam forms the diffraction pattern in the back focal plane of the objective lens which is then magnified by projector lenses to form the final diffraction pattern on the screen, and the selected area electron diffraction (SAED) pattern of sample is obtained. The SAED provides the lattice constants, orientation and other crystallographic information of the crystalline sample. The TEM used in this work was TEM-FEI "Technai 20U Twin with EDX and Technai 20G2 operated at 200KeV".

2.6.4 Dielectric Spectroscopy

The dielectric permittivity of a material is used to know how easy it can be polarized by an applied electric field. The dielectric constant (relative permittivity) of material talks about its ability to store capacitive energy. The permittivity parameter contains the real and imaginary parts. The dielectric loss tangent (tan δ) is the ratio of the imaginary permittivity to the real permittivity. In present thesis work, the dielectric

permittivity, dielectric-loss and resistive behavior were measured at various frequencies with changing the temperature using Keysight-E4990A impedance analyzer. The dielectric capacitance of samples was measured in the parallel plate capacitor method. The sample is sandwiched between two electrodes of Ag- metal to form a capacitor. The capacitance is measured with varying the frequency and temperature. The dielectric permittivity is calculated from the measured capacitance. The capacitance and dielectric loss were measured in the frequency range 100 Hz to 1MHz for most of the characterized samples. The capacitance of parallel plate capacitor can be related as follows $C = \varepsilon A/d = \varepsilon_r \varepsilon_0 A/d$ where ε_r is relative permittivity of the dielectric material, ε_0 is the permittivity of free space, 'A' is area of electrode and 'd' is the thickness of dielectric in between the parallel electrode plates.

2.6.5 Polarization-Electric field hysteresis loop characterization

A ferroelectric material contains spontaneous polarization which is a basic condition for designing ferroelectric photovoltaic devices. The polarization-electric field (P-E) hysteresis loop is measured to know the ferroelectric behaviour of materials. The P-E hysteresis loop technique is based on the classic Sawyer-Tower circuit, as depicted in Fig. 2.20. During the P-E loop measurement, the voltage is cycled by a signal generator. In the Sawyer-Tower circuit, the ferroelectric capacitor (sample) is connected with in series with a reference capacitor. The polarization 'P' is found as P= Q/A = (C*V/A), where 'Q' is the charge on the capacitor, which is same on both capacitor as they are connected in series, 'A' is the area of electrode area of sample and 'V' is the voltage across the reference capacitor, which is measured with an oscilloscope. From P-E loop, the remnant polarization and coercive field can be acquired. In this work, the ferroelectric polarization as a function of external field was

examined by Precision Premier-II ferroelectric tester from Radiant Technologies, USA. The P-E hysteresis loops were recorded at room temperature and also with varying the temperatures. The P-E loops are measured with varying the frequencies in the range 1Hz to 1kHz with a sinusoidal ac-voltage.

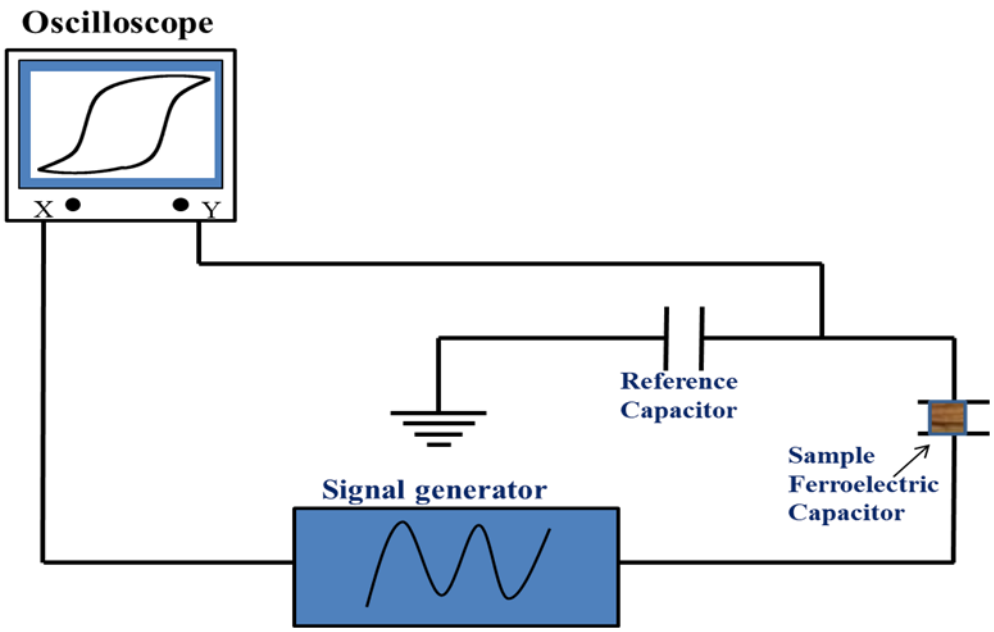

Figure 2.20 Schematic Sawyer-Tower circuit for measurement of ferroelectric polarization.

2.6.6 UV- Visible spectroscopy

The UltraViolet-visible (UV-Vis) absorbance spectra of materials are recorded by using Spectrophotometer and the optical band gap is calculated by well-known Tauc equation [J. Tauc (1968)]. The optical band gap is estimated from the Tauc relation $(\alpha h\nu)^2 = A(h\nu - E_g)$ where α is absorbance coefficient, E_g is optical band gap, 'h' is plank's constant and 'ν' is frequency [J. Tauc (1968)]. In the present thesis, we have

used Horiba Jobin Yvon spectrophotometer to record the UV-Vis. spectra of various samples.

2.6.7 Raman Spectroscopy

Raman spectroscopy is another important technique to analyze the chemical and structural properties of materials. Raman spectroscopy is a type of molecular spectroscopy that is based on Raman Effect discovered by C.V. Raman [C.V. Rman et al (1928)]. It is based on the inelastic scattering of incident photon radiation. The Raman Effect is defined as "frequency of a small fraction of scattered radiation is different from frequency of monochromatic incident radiation". A Raman spectrometer consists of a laser light source, spectrometer and a sampling interface. During measurement, materials are illuminated with a monochromatic laser beam. The interaction of laser beam with the molecules of sample results in scattered light which has different frequencies and thus Raman spectra arises. Raman spectra for the present thesis work were recorded using [WITec GmbH, Germany] spectrophotometer with 532 nm laser excitation wavelength.

2.6.8 Atomic Force Microscopy and Piezoresponce Force Microscopy

Atomic force microscopy (AFM) technique is widely used advanced characterization method to investigate the surface morphology of the flat samples. An AFM unit consists of a cantilever with a silicon tip, a photo-detector, laser diode, scanner and feedback loop, as shown schematically in Fig.2.21. The tip is mounted at the end of cantilever. The AFM tips are made from silicon. When the tip approaches near the surface of sample, the inter-atomic forces between atom at sample surface and atom at AFM tip generates a measurable deflection of the cantilever. AFM measures the vertical deflection of the cantilever with picometer resolution. In this system, the laser

beam reflected from the backside of the AFM cantilever is detected on to a position sensitive photodetector to measure the AFM tip deflection. A slight deflection of the cantilever will tilt the reflected beam and change the position of beam on the photodetector. Images are created by recording the effects of the interaction forces between tip and specimen surface as the cantilever is scanned over the sample.

Kelvin probe microscopy (KPFM) is a multimode atomic force microscopy method for measuring local surface potential of films in nanoscale range. KPFM works in non-contact mode where a conductive tip scans a sample surface. Due to potential difference between tip and sample, the tip feels an electrostatic force that can be detected by means of a laser beam and a detector. The KPFM mode uses an electrically conductive probe and during the measurement two scans are taken per data acquisition line. In first scan surface topography is measured and in second scan surface potential data is acquired in lift mode [G. X. Xia et al. (2003)].

Piezoresponse force microscopy (PFM) is voltage-modulated scanning force microscopy which permit the detection and switching of ferroelectric domains at the nanoscale [G. A. Smolenskii et al. (1982)]. In PFM, an ac-voltage is applied between the bottom electrode of the sample and a conductive tip in order to excite a local piezoelectric response [C. Harnagea et al. (2006)]. During measurement, the piezoelectric contribution from sample is dominant and the electrostatic contribution can be neglected. The surface of the ferroelectric sample oscillates due to the converse piezoelectric effect, and thus, oscillations are directly transmitted to the cantilever [P. Guthner et al. (1992)]. This local deformation is retrieved from the deflection signal of the cantilever and used to construct the ferroelectric domain image [C. Harnagea et al. (2006)]. The surface morphology of thin films was visualized by using Atomic Force Microscopy (AFM). The AFM imaging was carried out on an NT-MDT, NTGRA

Prima (Russia) system using a Pt-coated cantilever tips (NSG01) with a tip curvature radius of 40 nm. We have investigated the surface potential of films by Kelvin probe force microscopy (KPFM). Both topography and surface potential were measured simultaneously in a single pass.

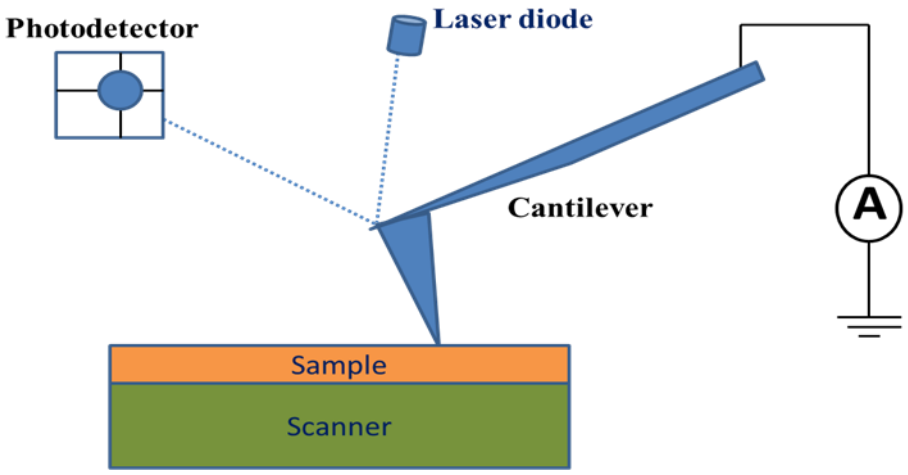

Figure 2.21 Schematic diagram of atomic force microscopy system.

2.6.9 Photovoltaic device Measurement

The current–voltage (I-V) characteristics of as prepared ferroelectric photovoltaic devices were measured using Keithley 2400 source- meter interfaced with a computer. A green laser light (wavelength ~ 532 nm, 5-50mW power) and visible light is used to illuminate the surface.

The current map and local I-V curve of film was recorded using C-AFM under light and dark. A green laser light (wavelength ~ 532 nm, 5 mW power) was used to illuminate the device surface. The photovoltaic properties of p-i-n heterojunction photovoltaic devices were investigated by performing the current-voltage measurements both in dark and under light illumination. Fig.2.22 shows the schematics of I-V measurement using C-AFM system.

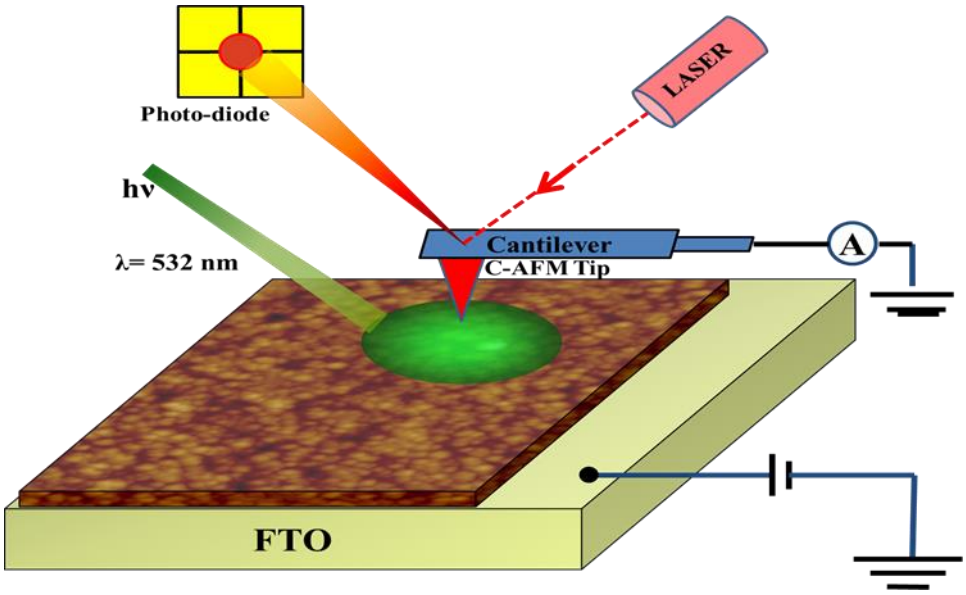

Figure 2.22 Schematic illustration of I-V measurement from C-AFM system.

2.7. Conclusions

This chapter briefly describes the preparation method used for bulk ceramics ferroelectric solid solutions, thin films by PLD, RF sputtering and chemical solution deposition by spin coating method. A brief description of various characterization techniques used in the present thesis is presented. The details of ferroelectric photovoltaic device fabrication and their characterization are also given. The subsequent chapters of these will present the important results of our investigations on various classes of ferroelectric photovoltaic materials.